MDPI

Article

Synthesis of Hydronium-Potassium Jarosites: The Effect of pH and Aging Time on Their Structural, Morphological, and Electrical Properties

Elías Hernández-Lazcano [1], E. Cerecedo-Sáenz [1], J. Hernández-Ávila [1], Norman Toro [2,3], T. V. K. Karthik [4], D. Mendoza-Anaya [5], M. E. Fernández-García [5], V. Rodríguez-Lugo [1,*] and E. Salinas-Rodríguez [1,*]

1 Academic Area of Earth Sciences and Materials, Institute of Basic Sciences and Engineering, Autonomous University of Hidalgo State, Highway Pachuca-Tulancingo km. 4.5, C.P., Hidalgo 42184, Mexico; elias.dezlaz@gmail.com (E.H.-L.); mardenjazz@yahoo.com.mx (E.C.-S.); herjuan@uaeh.edu.mx (J.H.-Á.)
2 Faculty of Engineering and Architecture, Universidad Arturo Prat, Almirante José Latorre 2901, Antofagasta 1244260, Chile; ntoro@ucn.cl
3 Departamento de Ingeniería Metalúrgica y Minas, Universidad Católica del Norte, Antofagasta 1270709, Chile
4 Higher School of Tepeji-Autonomous University of Hidalgo State, Noxtongo, Tepeji del Río de Ocampo, Hidalgo 42855, Mexico; krishnakarthik.tv@gmail.com
5 National Institute of Nuclear Research, Highway Mexico-Toluca S/N, La Marquesa, Ocoyoacan 52750, Mexico; demetrio.mendoza@inin.gob.mx (D.M.-A.); maria.fernandez@inin.gob.mx (M.E.F.-G.)
* Correspondence: ventura.rl65@gmail.com (V.R.-L.); salinasr@uaeh.edu.mx (E.S.-R.); Tel.: +52-2225-695-166 (V.R.-L.); +52-7712-074-171 (E.S.-R.)
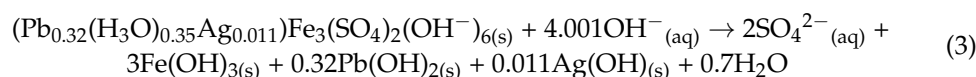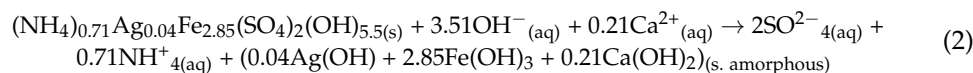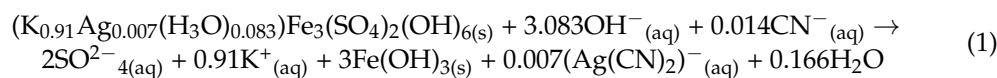
Abstract: Structural and morphological properties of hydronium-potassium jarosite microstructures were investigated in this work, and their electrical properties were evaluated. All the microstructures were synthesized at a very low temperature of 70 °C with a reduced reaction time of 3 h. An increase in the pH from 0.8 to 2.1 decreased the particle sizes from 3 μm to 200 nm and an increase in the aging time from zero, three, and seven days resulted in semispherical, spherical, and euhedral jarosite structures, respectively. The Rietveld analysis also confirmed that the amount of hydronium substitution by potassium in the cationic site increased with an increase in pH. The percentages of hydronium jarosite (JH)/potassium jarosite (JK) for pH values of 0.8, 1.1, and 2.1 were 77.72/22.29%, 82.44/17.56%, and 89.98/10.02%, respectively. Microstructures obtained in this work were tested as alternative anode materials and the voltage measured using these electrodes made with hydronium-potassium jarosite microstructures and graphite ranged from 0.89 to 1.36 V. The results obtained in this work show that with reduced particle size and euhedral morphology obtained, modified jarosite microstructures can be used as anode materials for improving the lifetime of lithium-ion batteries.

Keywords: hydronium jarosite; potassium jarosite; microstructures; pH; aging time; energy storage; euhedral morphology

1. Introduction

Mineralogically, jarosite belongs to the isostructural family of minerals "Jarosite-Alunite", in which the general formula is $AB_3(SO_4)_2(OH)_6$, where A can be, H_3O, Na, Rb, Ag, K, NH_4, $1/2Pb$, or $1/2Hg$, and B can be Al (III), Cu (II), or Fe (III). Thus, potassium jarosite is a hydrated mineral that contains alkalis and ferric iron with the chemical formula $H_3O\text{-}KFe_3(SO_4)_2(OH)_6$ [1–3]. Jarosite [$KFe_3(SO_4)_2(OH)_6$] is a pure mineral that belongs to the trigonal crystal system with a rhombohedral structure and has been be acquired from highly acidic surroundings such as in the southeast Spain, where jarosite was found for the first time in the Jaroso Ravine in the Almagrera Sierra [4]. Jarosite-type compounds have been of great interest mainly to mineralogists and metallurgists devoted to extractive metallurgy, because the jarosites contain valuable metals such as silver in their crystalline

structure, which can be recovered by alkaline decomposition processes [5], involved in the following chemical reactions: [6] Formula (1), [7] Formula (2), and [8] Formula (3)

$$(K_{0.91}Ag_{0.007}(H_3O)_{0.083})Fe_3(SO_4)_2(OH)_{6(s)} + 3.083OH^-_{(aq)} + 0.014CN^-_{(aq)} \rightarrow$$
$$2SO^{2-}_{4(aq)} + 0.91K^+_{(aq)} + 3Fe(OH)_{3(s)} + 0.007(Ag(CN)_2)^-_{(aq)} + 0.166H_2O \quad (1)$$

$$(NH_4)_{0.71}Ag_{0.04}Fe_{2.85}(SO_4)_2(OH)_{5.5(s)} + 3.51OH^-_{(aq)} + 0.21Ca^{2+}_{(aq)} \rightarrow 2SO^{2-}_{4(aq)} +$$
$$0.71NH^+_{4(aq)} + (0.04Ag(OH) + 2.85Fe(OH)_3 + 0.21Ca(OH)_2)_{(s.\ amorphous)} \quad (2)$$

$$(Pb_{0.32}(H_3O)_{0.35}Ag_{0.011})Fe_3(SO_4)_2(OH^-)_{6(s)} + 4.001OH^-_{(aq)} \rightarrow 2SO_4{}^{2-}_{(aq)} +$$
$$3Fe(OH)_{3(s)} + 0.32Pb(OH)_{2(s)} + 0.011Ag(OH)_{(s)} + 0.7H_2O \quad (3)$$

During the elimination of iron in the leaching process, where the residues have to be filtered and discarded, jarosite [9] has been predominantly used where the particle size and morphology play a crucial role. Large particle sizes are always preferred to improve the filtering process [10]. Other important applications of nano- or microstructured potassium jarosite $[KFe_3(SO_4)_2(OH)_6]$ are spin chirality on a two-dimensional (2D) geometrically frustrated lattice, geochemical indicators due to their unique structural and magnetic properties [11,12].

In addition, jarosite is a mineral that is found all over the planet and has been detected in Mars [13]. This mineral can be found in acidic sulfate soils, and oxidized zones of sulfur mineral deposits. In the industry, it can also be found in hydrometallurgical and bioleaching systems, and in environments contaminated by acid mine drainage [14]. It has also been proven that jarosite-type compounds are better absorbents of dangerous wastes as compared with other minerals for the elimination of toxic metals, due to the presence of these toxic elements in the crystalline structure of the jarosite-type compounds [15], such as Cr [16], V [17], Pb-As, Pb-Cu and Pb-Zn [18], As [19], and Pb [8].

For decades, the properties of this mineral, as well as the conditions of synthesis and decomposition, have been studied widely, principally employed in the zinc industry process to precipitate non-desired iron and other elements and to facilitate the filtering process. Recently, however, studies on this mineral have been carried out as they have also provided information on the geochronology and climate of the area in which they are found. Due principally to the isotopic relationship of O and H in the OH groups, in hydronium jarosite (Formula (4)) and copiapite (Formula (5)), which together with schwertmannite (Formula (6)), are minerals that have hydroxyl groups in their structure due to their similar chemical structures as follows:

$$(H_3O)Fe_3(SO_4)_2(OH)_6 \quad (4)$$

$$Fe^{2+}(Fe^{3+})_4(SO_4)_6(OH)_2 \cdot 20H_2O \quad (5)$$

$$(Fe^{3+})_{16}O_{16}(OH)_{9.6}(SO_4)_{3.2} \quad (6)$$

Thus, these isotopic studies have helped to determine, important information about the geochemical processes that contribute to establish climatic and geochronological changes [15,20,21].

A wide range of researchers have carried out experiments to synthesize jarosite under laboratory conditions (synthetic jarosite) where the principal characteristics employed during the synthesis were high synthesis temperatures (>90 °C) and time (>24 h) [5–8]. For example, alkaline decomposition of jarosite-type compounds obtained with synthesis temperatures between 93 and 98 °C and time of ~24 h has been executed, where the particle sizes were from 20 to 80 µm in diameter [8,17,19,22,23]. Additionally, synthesis of jarosite particles with diameters <50 nm has been reported, however, the presence of other agents such as potassium fluoride, δ-MnO_2 nanosheets, and other variables were necessary during the synthesis in addition to the traditional wet chemical method [17,24,25]. Until now, different synthesis methods have been developed with different parameters for obtaining jarosite structures, but the wet chemical synthesis method is the most sim-

ple, precise, and cost-effective method for obtaining size and morphologically-controlled jarosite microstructures [16].

Traditionally, jarosites have been synthesized to eliminate Fe from a hydrometal-lurgical solution from electrolytic zinc recovery, and other applications; however, recent investigations have paid attention to the use of this type of compounds as anodes and/or cathodes in lithium-ion batteries. A scalable method to prepare a two-dimensional material composed of a hybrid material of potassium jarosite/rGO, has been proposed for using jarosite as a cathode. This is a solution phase oxidation process at elevated temperature, where the grapheme oxide sheets act as a base for the direct growth of mono crystals of potassium jarosite [25]. The $KFe_3(SO_4)_2(OH)_6$/rGO hybrid material synthesized has been demonstrated to have significant potential for applications such as a high-performance cathode material in new-generation lithium-ion rechargeable batteries. Therefore, potassium jarosite ($KFe_3(SO_4)_2(OH)_6$ and sodium jarosite [$NaFe_3(SO_4)_2(OH)_6$] materials have attracted the attention of researchers for their application as cathodes in lithium-ion batteries, due to their unique topotactic reversible reaction [9]. In this electrochemical process, jarosite-type hydrosulfates have indicated their energy storage capability [9]. In the same way, Ding et al. [26] used a template-assisted redox method to synthesize nanosheets of potassium jarosite that delivered a large specific capacity of 117 mA h g^{-1} at 0.2 C and about 80 mA h g^{-1}, at 10 C, after 50 cycles, and showed excellent rate capability and capacity retention.

Other researchers have highlighted that the crystalline structure of these compounds, the alkaline elements involved such as K and Na, and the morphology played an important role in the intercalate and deintercalate of small ions such as Li^+ between the layers. Theoretically, there are three lithium ions that can be intercalated and deintercalted, as mentioned in the formula, $KFe_3(SO_4)_2(OH)_6$. In the jarosite crystal structure, the potential range of 1.5–4 V vs. Li/Li^+, via reduction/oxidation between Fe^{3+} and Fe^{2+}, corresponds to a theoretical capacity of 166 mA h g^{-1}, which makes it a promising cathode material for lithium-ion batteries (LIBs) [2,27–29].

All the above studies and others related to jarosite-type compounds have managed to find interesting advanced innovation for obtaining these materials, which by modifying parameters and synthesis methods have found appropriate morphologies and particle sizes to evaluate new properties that place them as a material with possible applications in new fields such as that of energy storage. Currently, the field of portable electronics continues to be monopolized by first-generation $LiCoO_2$ layered cathodes in lithium-ion batteries (LIBs) and recent research has favored removing Co, due to its toxicity and method of obtaining. For this reason, they are looking for new materials that have a low cost with great capacity to behave either as an anode or cathode [30–32].

Therefore, this work demonstrates the improvements such as low operation temperature (70 °C), low synthesis time (3 h), changes in pH, and aging time applied to the traditional method of synthesis for jarosite-type compounds to obtain a new modified method making the synthesis both economical and environmentally friendly. Changes in pH (0.8, 1.2, and 2.1) and the aging time (zero, three, and seven days) after the synthesis, have contributed significantly to a reduction in particle size and the morphologies such as spherical and euhedral. Some authors have indicated that the high crystalline structure of a jarosite-type compound, its particle size, and morphology have significant impact on the lifecycle and experimentally achievable capacity for the galvanostatic charge-discharge in LIBs [33]. Finally, the obtained synthetic jarosite structures could be utilized as a novel material in lithium-ion batteries according to the results found in the Daniell Cell for the electrodes made of jarosite and graphite.

2. Materials and Methods

2.1. Synthesis of Hydronium-Potassium Jarosite

In this work, first the synthesis method was modified to find the best experimental conditions to obtain jarosite-type compound with reduced particle size, and then by fixing

the parameters the process was directed to modify the morphology to analyze the electrical properties of these powders. The synthesis of potassium jarosite employed in this work was similar to the method reported by Dutrizac and Kaiman [34] and Salinas et al. [22] with considerable modifications. In addition, all chemicals, iron (III) sulfate ($Fe_2(SO_4)_3$) and potassium sulfate (K_2SO_4) as a source of potassium jarosite and sodium hydroxide (NaOH) and sulfuric acid, (H_2SO_4) were utilized for adjusting pH in this work and were purchased from Sigma-Aldrich (St. Louis, MO, USA) with high purity (>99%). In the present work, 0.15 M of $Fe_2(SO_4)_3$ and K_2SO_4 aqueous solutions were separately prepared in 0.5 L three-neck flasks containing a mixture of $Fe_2(SO_4)_3$ and K_2SO_4 in 0.3 L deionized water equipped with a pH measurement system, with the temperature maintained at 70 °C. Figure 1 shows the experimental setup for obtaining the jarosite powders.
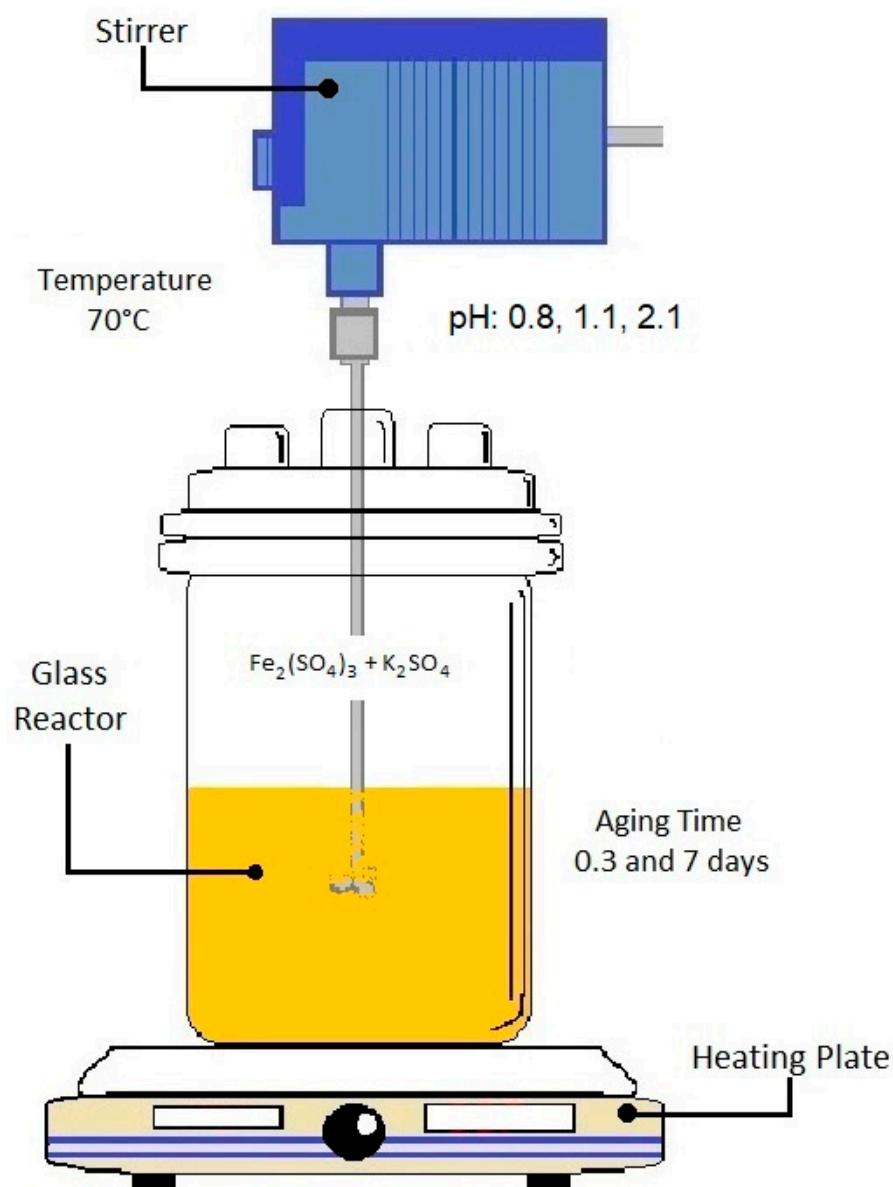

Figure 1. Experimental apparatus mounted to synthesize the potassium jarosite.

The above mixed solution had a pH of 1.1 and it was left for 3 h with a stirring rate of ~200 s^{-1}, which resulted in brown precipitates. The procedure was replicated for samples with a pH of 0.8 and 2.1 by adding H_2SO_4 and NaOH, respectively, drop wise through the left neck of the flask and monitoring the pH with a potentiometer placed in the right neck of the flask. The reaction time of ~3 h, synthesis temperature of ~70 °C, and stirring

rate of 200 s^{-1} were kept constant for all the samples. Finally, precipitates, in each case, were collected separately, filtered, and dried at room temperature. Additionally, two more samples with pH of 2.1 were synthesized with an additional aging time of 3 and 7 days before the filtration of precipitates. All the samples synthesized are shown in Table 1.

Table 1. List of samples with their synthesis conditions studied in this work.

Sample Name	pH	Aging Time
Jar-0.8-0	0.8	0
Jar-1.1-0	1.1	0
Jar-2.1-0	2.1	0
Jar-2.1-3	2.1	3
Jar-2.1-7	2.1	7

2.2. Material Characterization

All the synthetic jarosite powders were characterized by low-vacuum scanning electron microscopy (LV-SEM) in a JEOL JSM5900-LV machine equipped with an Oxford energy dispersive spectrometry (EDS) and operated at 20 kV to observe surface morphology, chemical composition, and the effect of pH and sintering temperature on particle size. The X-ray diffraction analysis was carried out using the powder technique in a Bruker D8 Discover diffractometer, with a CuKα = 1.5406 Å radiation source, operating at 40 kV and 40 mA. Diffraction patterns were collected in a 2θ range from 10° to 70° with an increment step size of 0.03° to identify the phase compound and the crystalline structure of jarosite. Finally, the X-ray diffraction patters were subjected to a Rietveld analysis using a Topas^2 software; R^{3e} factor and χ^2 were parameters used to indicate the accuracy of this refinement of X-ray diffraction (XRD) patterns.

2.3. Preparation of Electrodes and Evaluation of Electrical Conductivity

To evaluate the electrical properties of the powders of hydronium-potassium jarosite, electrodes of a mixture of jarosite and graphite were prepared. The procedure to elaborate the electrodes was the following: First, 0.1 g of graphite was weighed for each electrode and, from each jarosite sample, 0.1 and 0.5 g were weighed, respectively, to obtain two electrodes from each sample. Then, 15 to 20 drops of silicone oil were added with a syringe to form the paste, which was subsequently deposited on a piece of transparent plastic acetate that served as a mere support for the paste, as shown in Figure 2.
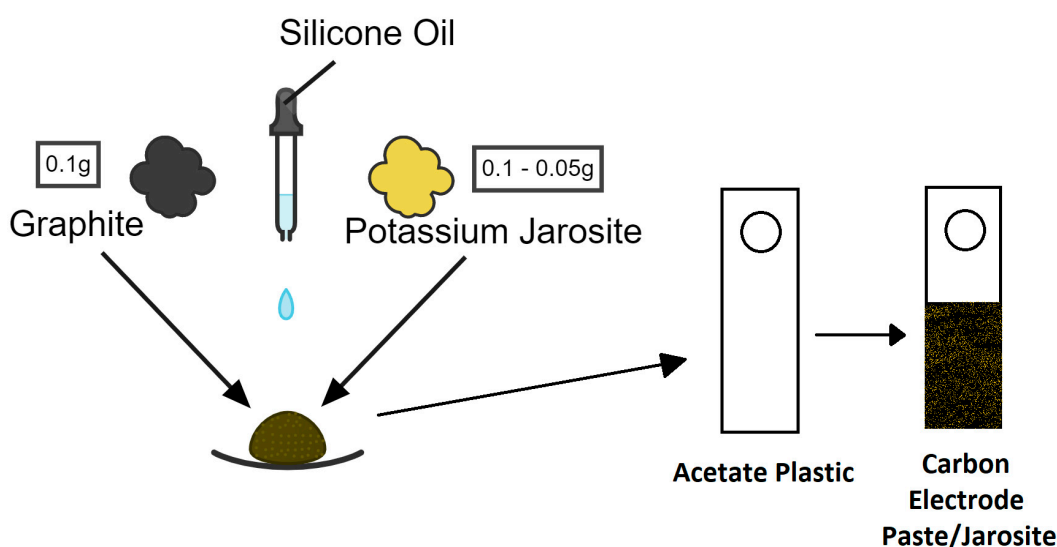

Figure 2. Elaboration of the electrodes for the evaluation of the electrical properties of jarosite.

To carry out the electrical tests of the hydronium-potassium jarosite samples, an arrangement similar to the one shown in Figure 3 was setup, and the tests were carried out with calcium chloride (CaCl$_2$) as electrolyte in order to evaluate the behavior of the electrodes.
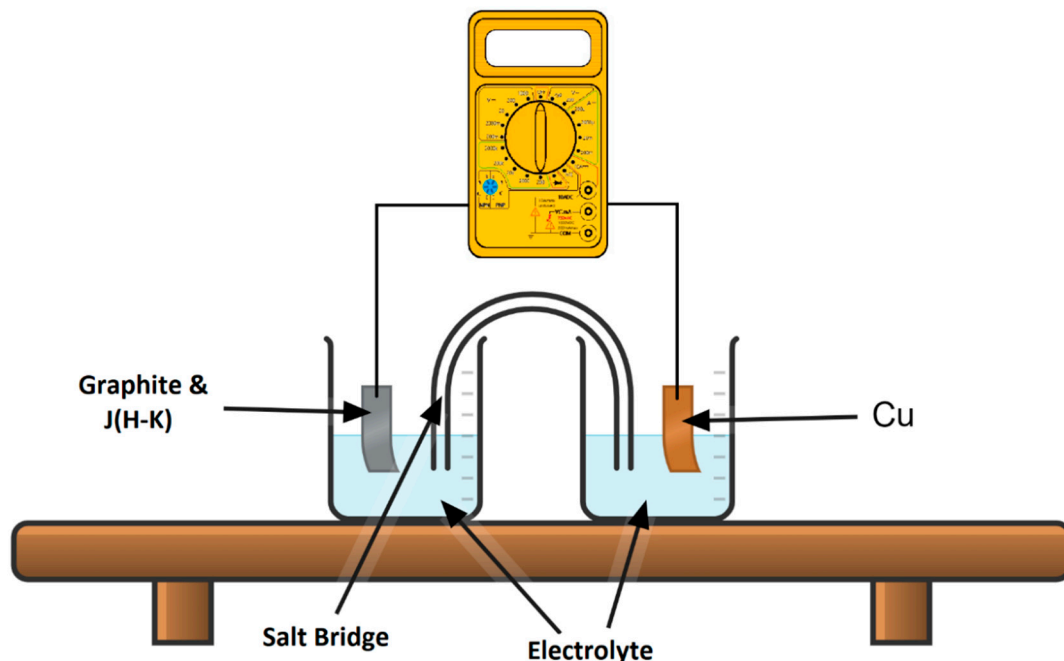

Figure 3. Experimental arrangement for electrical tests (Daniell's Cell).

For the electrical tests, a supersaturated solution (60 mL) of calcium chloride (CaCl$_2$) in injectable water was prepared to be used as electrolyte, a Cu coin was used as cathode, and the different electrodes were prepared with paste of carbon + jarosite synthesized at different pH's.

3. Results and Discussion

3.1. X-ray Diffraction (XRD) Analysis

The X-ray diffraction patterns of the synthesized potassium jarosite powders for all samples are shown in Figure 4. The patterns show the formation of synthetic potassium jarosite (H$_3$O-K)Fe$_3$(SO$_4$)$_2$(OH)$_6$ with (113) as the preferential orientation. It is evident from Figure 4 that all the powders exhibit the rhombohedral structure of potassium jarosite and match the International Centre for Diffraction Data Powder Diffraction Files (ICDD PDF 22-0827). All samples synthesized with different pH values and aging times showed a well-defined crystallinity, and no other peaks related to different jarosite forms, or products related to precursor residues could be identified; therefore, a solid solution of hydronium-potassium jarosite powders was synthesized.

A comparison of all the XRD patterns showed that irrespective of aging time, all the diffraction peaks were narrow and well separated with an increase in pH, confirming that samples improved their crystallinity and increased crystallite size (Table 2) due to the reduction in strain and defect density of the crystal. Whereas an increase in the aging time made the diffraction patterns broader and connected. As shown in Figure 4, it is evident that with an increase in the aging time, intensities of all the planes decrease and planes such as (003), (015), (006), (027), and (009) try to vanish, which is corroborated by an increase in the chemical reactivity among the species involved, resulting in decomposition of the jarosite structures in the presence of the ionized residues after the precipitation with increased aging time. With an increase in the pH of the samples, there was no differences in the plane intensities or in the number of planes.
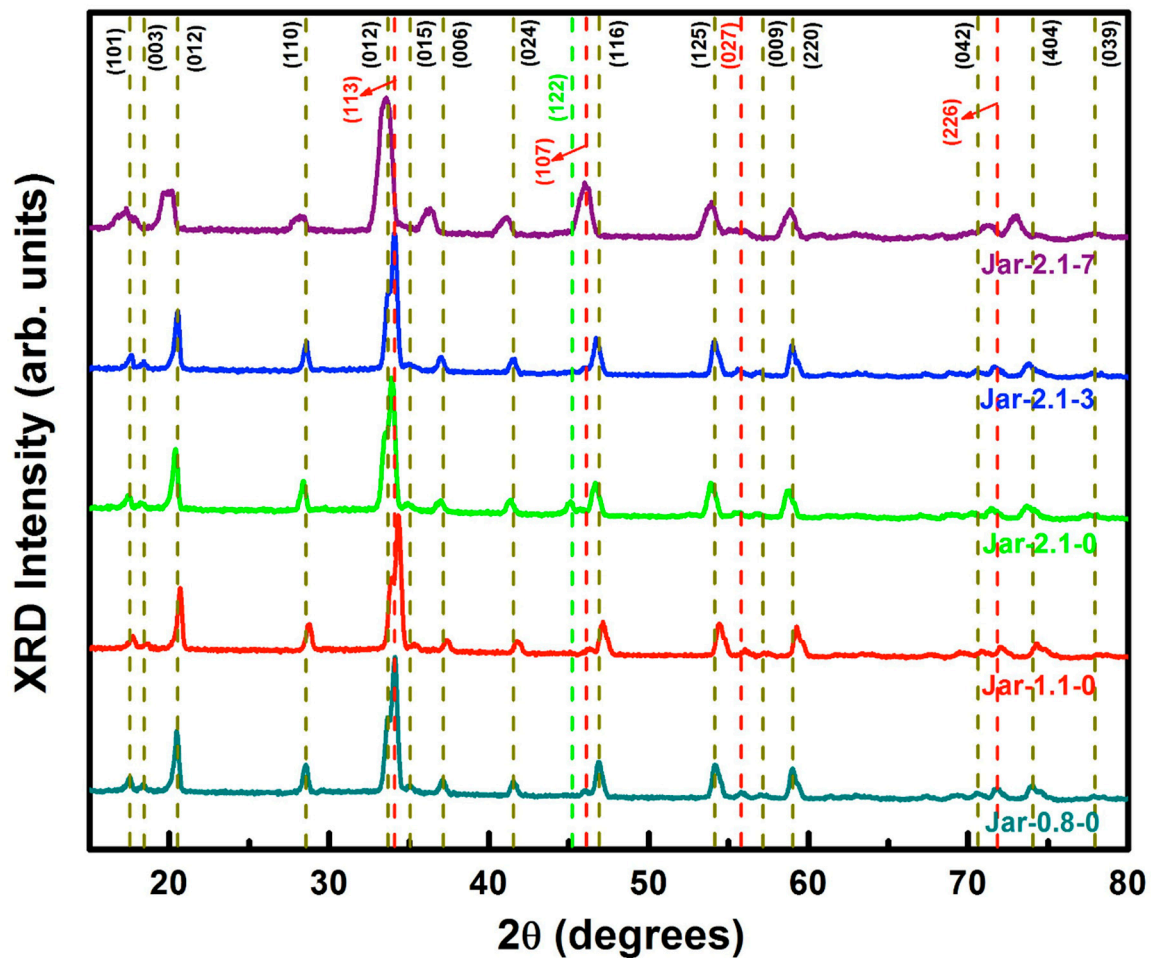
Figure 4. The X-ray diffraction (XRD) spectrums for samples synthesized at different pH values of 0.8 (Jar-0.8-0), 1.1 (Jar-1.1-0), and 2.1 (Jar-2.1-0), and aging time of 0 days (Jar-2.1-0), 3 days (Jar-2.1-3), and 7 days (Jar-2.1-7).

Table 2. Crystallite size and lattice parameters of jarosite powders for different aging times and pH values.

Sample Name	Average Crystallite Size (nm)	a (nm)	c (nm)
Jar-0.8-0	14.5	7.316	17.15
Jar-1.1-0	12.2	7.2995	17.12
Jar-2.1-0	9.48	7.2748	17.10
Jar-2.1-3	10.67	7.2837	17.12
Jar-2.1-7	7.83	7.2684	17.07
ICDDPDF 22-0827	-	7.29	17.13

Standard deviation 2.286 and medium size of crystallite 10.94.

The presence of precipitates during the aging makes the structures react with the released ions such as H_3O^+, K^+, Fe^{3+}, and OH^-, which restricts the growth in the desired planes or vanishes some planes. We believe that the presence of adequate OH- ions for the pH value 2.1 resulted in lower crystallite size and deviated lattice parameters.

In addition, with an increase in both pH and aging time, there is shift in the principle (113) plane for all jarosite structures, which is replotted and shown in Figure 5. In order to ascertain the effect of pH and aging time, a line broadening analysis of (113) peak using the Debye–Scherrer equation was employed to find the crystallite size and lattice parameters for all samples, as tabulated in Table 2.
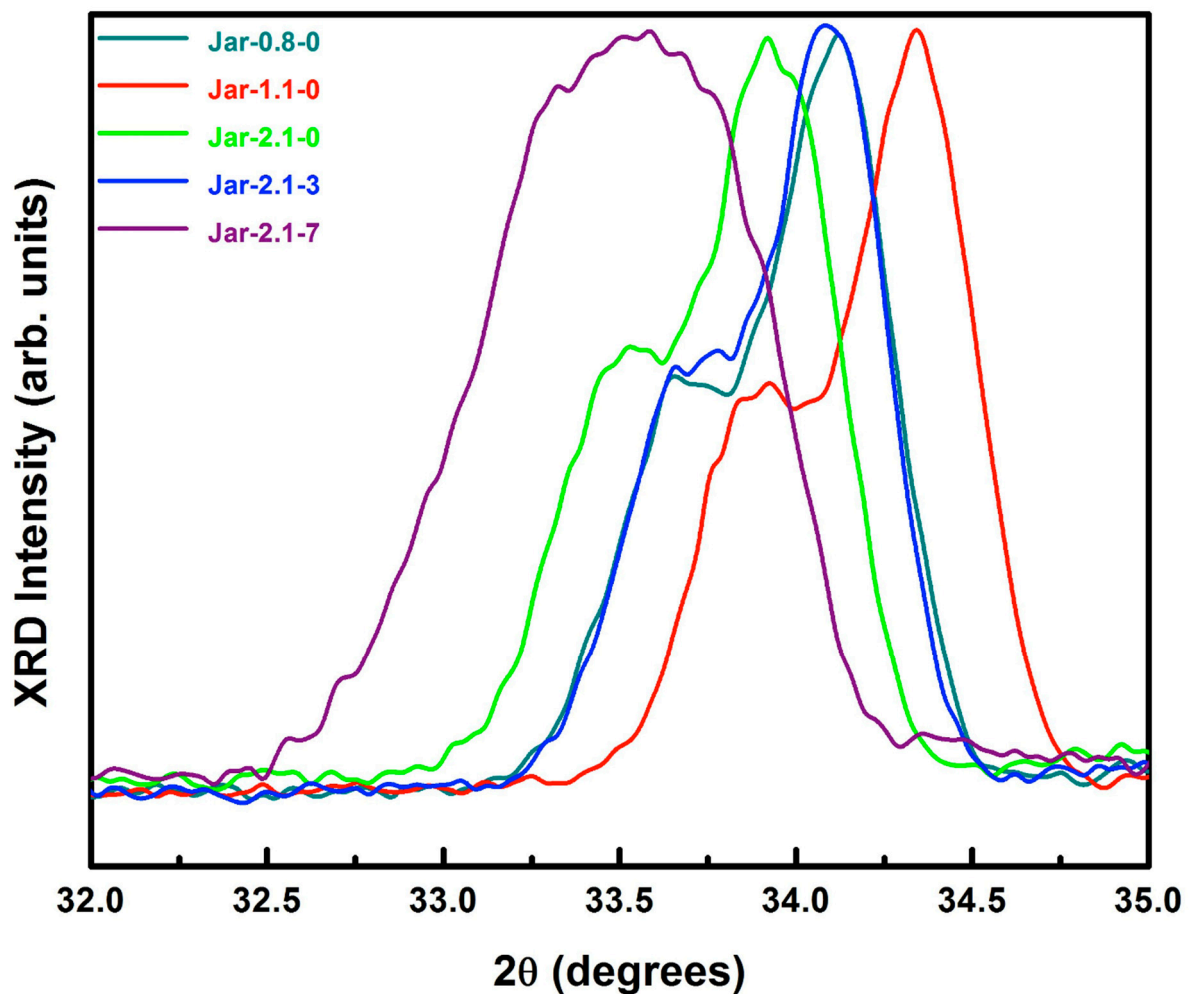
Figure 5. XRD (113) peak shift for all potassium jarosite structures.

By comparing Table 2 and Figure 5, it is evident that a decrease in pH from 1.1 to 0.8 increased the crystal size and lattice parameters showing a right shift, due to the substitution of hydronium by the potassium cation occurring in the jarosite structures. Whereas an increase in pH from 1.1 to 2.1 reduced the crystal size and lattice parameters, noting that a left shift in the preferential orientation occurred due to the above mentioned. Additionally, with an increase in the aging time from zero to three and seven days, a peak broadening, i.e., a shift in the (113) peak and vanishing of (012) plane, is noticed. Powders synthesized without any modification, utilizing sulfuric acid or ammonium hydroxide with pH of 1.1, present lattice parameters that are inconsistent with the theoretical synthetic jarosite lattice parameters. Whereas the lattice parameters are largely deviated for the aged powders and slightly deviated for the powder with different pH values. Crystallite size and lattice parameters decrease drastically for powders with seven days aging time. This is due to the decomposition of the planes of the jarosite structures and the hydronium substitution produced during the decomposition of the planes in the aged powders. This clearly evidences that the pH and aging time causes significant hydronium substitution in the jarosite structure, which results in changes of the crystal size and lattice parameters.

Because NaOH was used to control pH values, a Rietveld analysis was done (as described in Section 2.2) to determine if sodium jarosite was formed during synthesis. Table 3 shows the Rietveld results, it can be observed that only the potassium jarosite was formed with important substitution of hydronium, resulting in a solid solution of hydronium-potassium jarosite. In conclusion, it can be observed that with increasing pH

the amount of hydronium substitution also increases from 77.71% at a pH of 0.8 to 89.98% at a of pH 2.1.

Table 3. Rietveld analysis for the synthesis of jarosite and effect of pH values (0.8, 1.1, and 2.1).

Sample Name	Potassium Jarosite (JK) (%)	Lattice Parameters		Hydronium Jarosite (JH) (%)	Lattice Parameters	
		a (nm)	c (nm)		a (nm)	c (nm)
Original	-	7.2900	17.1600	-	7.3238	17.005
Jar-0.8-0	22.29	7.3840	17.0320	77.71	7.3238	17.005
Jar-1.1-0	17.56	7.3105	17.2731	82.44	7.3287	17.005
Jar-2.1-0	10.02	7.2913	17.1744	89.98	7.3052	16.9700

3.2. Scanning Electron Microscopy (SEM) and Energy Dispersive Spectrometry (EDS) Analysis

Scanning electron microscopy (SEM) and energy dispersive spectrometry (EDS) were employed to obtain the morphological and compositional properties of the jarosite powders and subsequently interpret their association with the structural properties. Figure 6 shows the SEM images of the potassium jarosite powders synthesized at pH values of 0.8 (Figure 6a,b), 1.1 (Figure 6c,d), and 2.1 (Figure 6e,f); aged for zero (Figure 6e,f), three (Figure 6g,h), and seven (Figure 6a,b) days. The EDS analysis of all the samples are resumed and tabulated in Table 3.

Jarosite powders show similar agglomerates of ~2 μm, for samples prepared with pH values 0.8 and 1.1 (see Figure 6a–d). The prepared powders with a pH of 1.1 show a dense morphology with a very broad distribution of grain size ranging from 500 nm to 3 μm (Figure 6c,d). A decrease in pH to 0.8 by adding sulphuric acid resulted in a decrement in the size of the agglomerates and also in the density of the particles (Figure 6a,b). This is attributed to the relative reduction in OH^- ion concentration. In both samples with pH values 0.8 and 1.1, no specific morphology was observed, only agglomerates with random size and density were noticed. As the pH value increased to 2.1, exceptionally, jarosite particles were observed with an elliptical or semi-spherical morphology with particle size around 1 μm (Figure 6e,f). For powders with a similar pH of 2.1 and with increased aging time of three and seven days, the morphology changed drastically to spherical and euhedral structures, respectively (Figure 6g–j). Particle sizes of around 500 and 200 nm were found for powders aged for three and seven days, respectively. Particle size decreased with an increase in aging time from 2 μm to 200 nm. By comparing the particles sizes analyzed in SEM with XRD crystallite sizes, we believe that the particles observed in SEM are constituted with smaller crystallites.

The prepared jarosite solution is acidic with pH 1.1 and as the pH of the solution is increased by the addition of a strong base, i.e., NH_4OH, mainly K^+ and OH^- ions are liberated which make the solution more soluble and these OH^- ions are situated on the facets of the formed nuclei [28]. Later the growth and agglomeration are restricted by OH^- ions resulting in some elliptical particles (Figure 6e,f). When the precipitates are left in the supernatant for three days, increased H_3O starts incorporating into the structure, allowing the growth in a direction, which results in the spherical-like morphology (Figure 6g,h). Furthermore, with an increase in the aging time to seven days, besides incorporation of the H_3O, a majority of the planes starts decomposing and forms particles with different facets resulting in euhedral potassium jarosite structures (Figure 6i,j). Therefore, pH is a very important parameter for obtaining the desired surface morphology. The decomposition of the planes is clear from the XRD analysis (Figures 4 and 5) where the planes (012) and (113) reduce to only (113), confirming the decomposition of planes and, subsequently, result in euhedral structures (Figure 6j). To observe the liberation and incorporation of cations and anions in each sample, EDS analysis was performed, and the results are tabulated in Table 4.
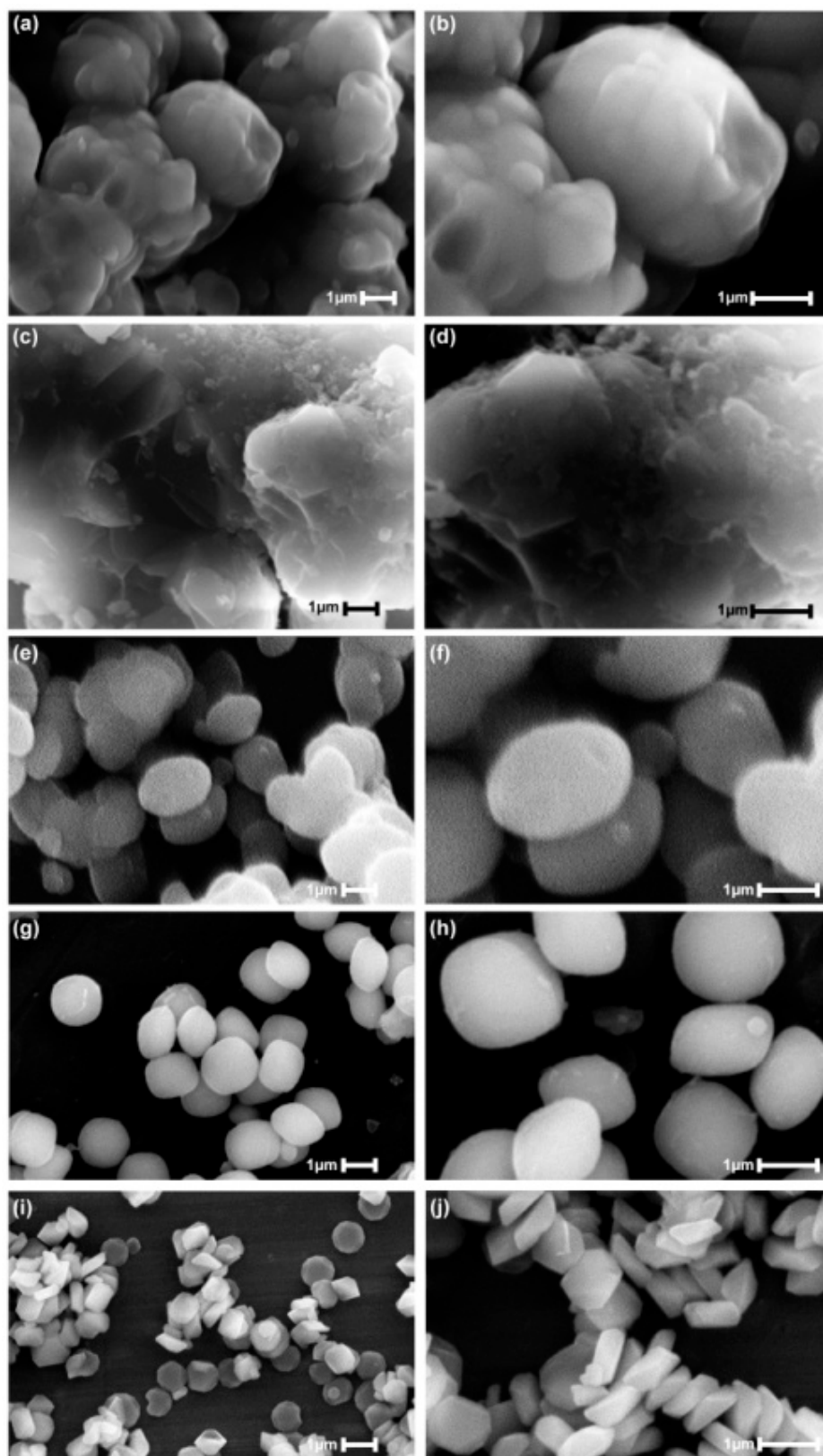
Figure 6. Scanning electron microscopy (SEM) image of potassium jarosite particles synthesized at different conditions. (**a**,**b**) pH 0.8; (**c**,**d**) pH 1.1; (**e**,**f**) pH 2.1 with no aging time; (**g**,**h**) pH 2.1 with 3 days aging time; (**i**,**j**) pH 2.1 with 7 days aging time. Left and right column images are with magnifications 10,000× and 20,000×, respectively.

Table 4. Energy dispersive spectrometry (EDS) point analysis of all the synthesized samples as compared with the theoretical and synthesized values reported [32].

Jarosite Component	Theoretical (%)	Synthetic (%)	Jar-0.8-0 (%)	Jar-1.1-0 (%)	Jar-2.1-0 (%)	Jar-2.1-3 (%)	Jar-2.1-7 (%)
K	7.81	7.17	5.50	6.20	6.72	7.02	7.15
Fe	33.45	29.50	20.20	20.90	21.20	21.48	21.43
SO_4	38.36	40.70	39.84	38.95	40.14	43.44	44.70
H_3O + OH *	20.38	22.63	34.56	33.95	31.94	28.06	26.72

* Calculated by difference and considering the incorporation of H_3O into jarosite structure.

In Table 4, we compare the elemental composition values with the theoretical and synthetic jarosite composition values reported by the traditional synthesis method employed first by Dutrizac and Kaiman who synthesized it simply by dissolving the corresponding alkali sulfate salt with ferric sulfate and heating at temperatures close to the boiling point of the solution, for reaction times ranging from 3 to 24 h [34]. According to the EDS results, it can be observed that the values of K and Fe are similar to the values reported from the traditional synthesis method with an increase in pH from 0.8 to 2.1, which we believe is due to the utilization of a lower molar concentration (0.15 M) as compared with the reported work. Whereas the contents of SO_4 and (H_3O + OH) were relatively higher which is conventional, because as the quantity of anions liberated increases, the solution pH also increases, and the pH utilized in the theoretical and synthetic jarosite was 1.2. Therefore, by comparing XRD, SEM, and EDS analysis it can be concluded that the aging time makes the jarosite form euhedral structures and increased pH makes the size of the particle more micrometric. The results of this work are preliminary and, in the future, detailed analysis of aging time and pH should be studied to obtain the nanometric jarosite structures.

3.3. Electrical Analysis

According to these results during electrical tests, it can be seen in Table 5 that the electrochemical reaction executed by the electrodes prepared with hydronium-potassium jarosite and graphite suggests that they are suitable as cathode materials. Table 5 shows that the best results found were for the jarosite synthesized at a pH of 2.1 with three and seven days of aging, where morphology is spherical and euhedral, respectively.

Table 5. Results obtained during the electrical test done on electrodes prepared with jarosite and graphite, using calcium chloride as electrolyte.

Electrode	Registry (V)	Reverse (V)
Cu coin	0.52	-
Graphite-0.1g (G1)	0.89	−0.90
G1/Jar-0.8-0 (0.1 g)	0.90	−0.95
G1/Jar)-0.8-0 (0.05 g)	0.90	−1.01
G1/Jar-1.1-0 (0.1 g)	0.96	−0.99
G1/Jar-1.1-0 (0.05 g)	0.89	−0.90
G1/Jar-2.1-0 (0.1 g)	0.94	−0.95
G1/Jar-2.1-0 (0.05 g)	0.90	−0.96
G1/Jar)-2.1-3 (0.1 g)	1.00	−1.00
G1/Jar-2.1-3 (0.05 g)	1.35	−1.42
G1/Jar-2.1-7 (0.1 g)	1.36	−0.98
G1/Jar-2.1-7 (0.05 g)	1.00	−1.05

According to these preliminary results, it can be seen that the jarosite synthesized at pH 2.1 and with a resting time of three and seven days, shows the best results, obtaining an average potential of 1.35 V, which is close to the potential generated by a standard battery that is 1.5 V and a little above the voltage generated by the rechargeable battery that is 1.2 V.

These results also indicate that particle size and morphology play an important role, since these materials have average particle sizes ranging from 1 to 0.2 microns, and spherical and euhedral morphologies (Figure 6g–j), which coincide with some researchers who have reported that particle size and morphology of crystalline jarosite played an important role in the ability of these compounds to serve as cathode in LIBs [9,34].

Finally, Table 6 shows the results found in this work as compared with other results from some previous research regarding the morphology, particle size, and electrical properties of these kind of solid solutions. It can be seen that the sizes and morphologies found were of importance during the electrical test carried out on these powders. In addition, the low temperature, pH, and reaction time used, combined with the aging time, resulted in these sizes and morphologies. Finding that with a pH of 2.1 and three to seven days of aging, the morphologies vary from spherical to euhedral with particle sizes from 0.2 to 1 μm.

Table 6. Comparative description of some previous works related to the synthesis of jarosite type compounds and their characteristics.

Jarosite	Synthesis Conditions/Results
K	25 °C, 1 atm, pH 0.9–2.22, time 6 weeks–6 months/potassium jarosite [35]
NH_3-Na	180–190 °C, 350 KPa, 0.75 h retention time/agglomerates >10 μm [36]
Ag-Pb	98 °C, 24 h, 500 s^{-1}/rhombohedral crystals, semispherical particles 80–100 μm [37]
K	99 °C, 24 h, 500 s^{-1}, pH 1.6/agglomerates [38]
Ag	98 °C, 24 h, jarosite seeds/semispherical particles >30 μm [6]
K-Na-H_3O	96 °C, 4 h, dehydrated overnight at 111 °C/ICDD PDF 220827 [15]
K	100 °C, 24 h, 500 s^{-1}, pH 1.5, dried at 283 K for 24 h/cauliflower particles >30 μm [39]
NH_4-H_3O-Ag	95 °C, 24 h, pH 1.8, using seeds to increase particle size/spherical particles of 37–44 μm [40]
K-F	70 °C, 48 h, dried 3 days at room temperature, pH 1.6/agglomerates of particles ~1 μm [24]
Ag-Rb	95 °C, 24 h, pH 1.2/particles 20–30 μm [22]
K-based GO	Graphene oxide layers, 81 °C, 12 h, stirred for 10 h at 25 °C/bulks of JK >10 μm, with nanoplates width ~800 nm and thickness ~100 nm, reversible capacity of 70.7 mAh g^{-1} [25]
K-rGO nanosheets	Dissolution of KNO_3-$FeSO_4 7H_2O$-GO, 111 °C (autoclave) during 12 h/particle size over 4 μm, 545 mAh g^{-1} at the end of 1000 cycles at 500 mAh g^{-1} [30]
H_3O-K	70 °C, 3 h, pH (0.8, 1.1 and 2.1), aging time 0, 3, and 7 days/particle sizes varying from agglomerates 5 to 10 μm to individual particles from 0.2 to 1 μm. Morphologies from quasi spherical, elliptical, spherical, and euhedral. With electrical properties generating from 0.86 to 1.36 V in the Daniell's cell (this work)

4. Conclusions

Wet chemical synthesis of potassium jarosite powders was successfully performed at a low temperature of ~70 °C and with only 3 h of reaction time. The results found in this work, indicate that the morphological and microstructural properties of hydronium-potassium jarosite have a strong dependency on synthesis parameters, mainly the pH of the solution and the aging time. For samples with a pH of 0.8 and 1.1, dense agglomerates around 3–2 μm were formed; with an increase in pH to 2.1, elliptical or nonspherical particles of ~1 μm were observed. Increasing the aging time from zero to three days resulted in pure spherical particles of ~500 nm. Furthermore, an increase in aging time to seven days obtained euhedral structures of ~200 nm. An increase in pH and aging time decreased the particle size and changed the morphology from elliptical to spherical and euhedral structures. The XRD patterns confirmed that all samples synthesized with the new method, were concordant with the ICDD PDF 20827 of the $(H_3O-K) Fe_3(SO_4)_2(OH)_6$ with a preferential orientation (113) plane with good crystalline structure. No other peaks related to different jarosite forms were identified. An increase in aging time confirms the decomposition of the planes, which is in good agreement with the SEM results. An increase in the pH released ions such as K^+, Fe^{3+}, and OH^-, which restricted the growth in desired planes or vanished some others, was also evidenced through the EDS analysis. As compared with theoretical and synthetic jarosite powders, the powders synthesized in this work are relatively a solid solution of hydronium-potassium jarosite with less particle size. In addition, the synthesis conditions utilized make the process easier and cost effective. The Rietveld analysis confirms that hydronium substitution by potassium in the alkaline site of the jarosite structure increase linearly with an increase in pH. Finally, based on the electrical measurements, jarosite powders obtained is this work can be utilized as new cathode material in lithium-ion battery applications, because the nominal voltage measured (1.3 V) is close to the standard battery (1.5 V) and a little above that of the rechargeable battery (1.2 V).

References

1. Das, G.K.; Anand, S.; Acharya, S.; Das, R.P. Preparation and decomposition of ammoniumjarosite at elevated temperatures in $H_2O(NH_4)_2SO_4H_2O$ media. *Hydrometallurgy* **1995**, *38*, 263–276. [CrossRef]
2. Drouet, C.; Navrotsky, A. Synthesis, characterisation and thermo-chemistry of K-Na-H_3O jarosites. *Geochim. Cosmochim. Acta* **2003**, *67*, 2063–2076. [CrossRef]
3. Smith, A.M.L.; Hudson-Edwars, K.A.; Dubbin, W.E.; Wright, K. Dissolution of jarosite [$KFe_3(SO_4)_2(OH)_6$] at pH 2 and 8: Insights from batch experiments and computational modelling. *Geochem. Cosmochim. Acta* **2006**, *70*, 608–621. [CrossRef]
4. Nuñez, C.; Roca, A. Concentration of Iron Oxides by Flotation from Gossan Ore Tailings. *Can. Metall. Q.* **1984**, *23*, 393–397. [CrossRef]

5.   Patiño, F.; Salinas, E.; Cruells, M.; Roca, A. Alkaline decomposition-cyanidation kinetics of argentian natrojarosite. *Hydrometallurgy* **1998**, *49*, 323–336. [CrossRef]

6.   Cruells, M.; Roca, A.; Patiño, F.; Salinas, E.; Rivera, I. Cyanidation kinetics of argentian jarosite in alkaline media. *Hydrometallurgy* **2000**, *55*, 153–163. [CrossRef]

7.   Patiño, F.; Cruells, M.; Roca, A.; Salinas, E.; Pérez, M. Kinetics of alkaline decomposition and cyanidation of argentian ammonium jarosite in lime medium. *Hydrometallurgy* **2003**, *70*, 153–161. [CrossRef]

8.   Patiño, F.; Flores, M.U.; Reyes, I.A.; Islas, H.; Reyes, M.; Juárez, G. Kinetic Modeling of the Alkaline Decomosition and Cyanidation of Argentian Plumbojarosite. *J. Mex. Chem. Soc.* **2014**, *58*, 3–10.

9.   Ding, Y.L.; Wen, Y.; Chen, C.C.; van Aken, P.A.; Maier, J.; Yu, Y. Nanosheets of earth-abundant jarosite as novel anodes for high-rate and high-life lithium-ion batteries. *ACS Appl. Mater. Interfaces* **2015**, *7*, 10518–10524. [CrossRef]

10. Hudson-Edwards, K.A.; Smith, A.M.L.; Dubbin, W.E.; Bennettt, A.J.; Murphy, P.J.; Wright, K. Comparison of the structures of natural and synthetic Pb-Cu-jarosites-type compounds. *Eur. J. Miner.* **2008**, *20*, 241–252. [CrossRef]

11. Salinas, E.; Roca, A.; Cruells, M.; Patiño, F.; Córdoba, D.A. Characterization and alkaline decomposition-cyanidation kinetics of industrial ammonium jarosite in NaOH media. *Hydrometallurgy* **2001**, *60*, 237–246. [CrossRef]

12. Hudson-Edwards, K.A.; Smith, A.M.L.; Dubbin, W.E.; Wright, K. Jarosite in acid mine drainage environments: Formation, mineralogy, stability. In Proceedings of the 15th Annual V. M. Goldschmidt Conference, Moscow, ID, USA, 20–25 May 2005; p. A765.

13. Salinas, E.; Reyes, M.; Patiño, F.; Méndez, M.T.; Rivera, I.; Martínez, A.; Hernández, L. Factores que afectan el crecimiento de partículas de jarosita de amonio argentífera sintética. *Rev. Soc. Quim. Mex.* **2002**, *46*, 67–72. (In Spanish)

14. Farrand, W.H.; Glotch, T.D.; Rice, J.W., Jr.; Hurowitz, J.L.A.; Swayze, G.A. Discovery of jarosite within the Mawrth Vallis region of Mars: Implications for the geologic history of the region. *Icarus* **2009**, *204*, 478–488. [CrossRef]

15. Kerolli-Mustafa, M.; Fajković, H.; Rončević, S.; Ćurković, L. Assessment of metals risks from different depths of jarosite tailing waste of Trepça Zinc Industry, Kosovo based on BCR procedure. *J. Geochem. Explor.* **2015**, *148*, 161–168. [CrossRef]

16. Mireles, I.; Reyes, I.A.; Flores, V.H.; Patiño, F.; Flores, M.U.; Reyes, M.; Acosta, M.; Cruz, R.; Gutierrez, E.J. Kinetics analysis of the decomposition of the $KFe_3(SO_4)_{2-x}(CrO_4)_xOH)_6$ jarosite solid solution in $Ca(OH)_2$ medium. *J. Braz. Chem. Soc.* **2016**, *27*, 1014–1025.

17. Zhao, R.; Li, Y.; Chan, C.K. Synthesis of jarosite and Vanadium jarosite analogues using microwave hydrothermal reaction and evaluation of composition-dependent electrochemical properties. *J. Phys. Chem. C* **2016**, *120*, 9702–9712. [CrossRef]

18. Forray, F.L.; Smith, A.M.L.; Navrotsky, A.; Wright, K.; Hudson-Edwards, K.A.; Dibbin, W.E. Synthesis, characterization and thermochemistry of synthetic Pb-As, Pb-Cu and Pb-Zn jarosites. *Geochim. Cosmochim. Acta* **2014**, *127*, 107–119. [CrossRef]

19. Patiño, F.; Reyes, I.A.; Flores, M.U.; Pandiyan, T.; Roca, A.; Reyes, M.; Hernández, J. Kinetic modeling and experimental design of the sodium aresenojarosite decomposition in alkaline media: Implications. *Hydrometallurgy* **2013**, *137*, 115–125. [CrossRef]

20. Drouet, C.; Pass, K.L.; Baron, D.; Draucker, S.; Navrotsky, A. Thermochemistry of jarosite-alunite and natrojarosite-natroalunite solid solutions. *Geochim. Cossmochim. Acta* **2004**, *68*, 2197–2205. [CrossRef]

21. Alvarado, A.; Velasco, F. Isótopos Estables en los Minerales de Drenaje Acido del Yacimiento de San Miguel (Faja Pirìtica Ibérica). *Rev. Soc. Española Miner.* **2008**, *9*, 27–28. (In Spanish)

22. Salinas, E.; Cerecedo, E.; Ramírez, M.; Patiño, F.; Pérez, M. Kinetics ok alkaline decomposition and cyanidation of argentian rubidium jarosite in NaOH medium. *Metall. Mater. Trans. B* **2012**, *43B*, 1027–1033. [CrossRef]

23. Perez-Labra, M.; Romero-Serrano, A.; Salinas-Rodriguez, E.; Avila-Davila, E.O.; Reyes-Perez, M. Synthesis, termo chemistry and kinetics of alkaline decomposition of rubidium jarosite in $Ca(OH)_2$ media. *Metall. Mater. Trans. B* **2012**, *43*, 773–780. [CrossRef]

24. Gunneriusson, L.; Sandström, A.; Holmgren, A.; Kuzmann, E.; Kovacs, K.; Vértes, A. Jarosite inclusion of fluoride and its potential significance to bioleaching of sulphide minerals. *Hydrometallurgy* **2009**, *96*, 108–116. [CrossRef]

25. Xu, W.; Xie, Z.; Cui, X.; Zhao, K.; Zhang, L.; Mai, L.; Wang, Y. Direct growth of an economic green energy storage material: Amonocrystalline jarosite-$KFe_3(SO_4)_2(OH)_6$—Nanoplates@rGO hybrid as a superior lithium-ion battery cathode. *J. Mater. Chem. A* **2016**, *10*, 3735–3742. [CrossRef]

26. Ding, Y.L.; Wen, Y.; van Aken, P.A.; Maier, J.; Yu, Y. Jarosite nanosheets fabricated via room-temperature synthesis as cathode materials for high-rate lithium ion batteries. *Chem. Mater.* **2015**, *27*, 3143–3149. [CrossRef]

27. Inami, T.; Nishiyama, M.; Maegawa, S.; Oka, Y. Magnetic structure of the *kagomé* lattice antiferromagnet potassium jarosite $KFe_3(SO_4)_2(OH)_6$. *Phys. Rev. B Condens. Matter Mater. Phys.* **2000**, *61*, 12181. [CrossRef]

28. Basciano, L.C.; Peterson, R.C. Crystal chemistry of the natrojarosite-jarosite and natrojarosite-hydronium jarosite solid-solution series: A synthetic study with full Fe site occupancy. *Am. Miner.* **2008**, *93*, 853–862. [CrossRef]

29. Nagano, H.; Taniguchi, I. Synthesis of $Li_2FeP_2O_7$/Carbon nanocomposite as cathode materials for Li-ion batteries. *J. Power Sources* **2015**, *298*, 280–284. [CrossRef]

30. Wu, N.; Tian, W.; Shen, J.; Qiao, X.; Sun, T.; Wu, H.; Zhao, J.; Liu, X.; Zhang, Y. Facile fabrication of a jarosite ultrathin $KFe_3(SO_4)_2(OH)_6$@rGO nanosheet hybrid composite with pseudocapacitive contribution as a robust anode for lithium-ion batteries. *Inorg. Chem. Front.* **2019**, *6*, 192–198. [CrossRef]

31. Qian, J.; Lui, L.; Yang, J.; Li, S.; Wang, X.; Zhuang, H.; Lu, Y. Electrochemical surface passivation of $LiCoO_2$ particles at ultrahigh voltage and its applications in lithium-based batteries. *Nat. Commun.* **2018**, *9*, 4918. [CrossRef]

32. Jiang, Y.; Qin, C.; Yan, P.; Sui, M. Origins of capacity and voltage fading of $LiCoO_2$ upon high voltage cycling. *J. Mater. Chem. A* **2019**, *7*, 20824–20831. [CrossRef]

33. Sandineni, P.; Asl, H.Y.; Choudhury, A. Kagomé lattices as cathode: Effect of particle size and fluoride substitution on electrochemical lithium insertion in sodium and ammonium jarosites. *J. Solid State Chem.* **2016**, *242*, 78–86. [CrossRef]
34. Dutrizac, J.E.; Kaiman, S. Synthesis and properties of jarosite type-compounds. *Can. Miner.* **1976**, *14*, 151–158.
35. Brown, J.W. A chemical study of some synthetic potassium-hydronium jarosites. *Can. Miner.* **1970**, *10*, 696–703.
36. Kunda, W.; Veltman, H. Decomposition of Jarosite. *Metall. Mater. Trans. B* **1979**, *10*, 439–446. [CrossRef]
37. Patiño, F.; Ramírez, J. Síntesis y caracterización de argentojarosita y plumbojarosita. *Rev. Soc. Quím. Mex.* **1993**, *37*, 51–62. (In Spanish)
38. Dutrizac, J.E.; Hardy, D.J. The behaviour of thiocyanate and the cyanate during jarosite precipitation. *Hydrometallurgy* **1997**, *45*, 83–95. [CrossRef]
39. Cadena, J.L.; Chimeros, J.M.; Queralt, I.; Viladevall, M.; Pérez, K.F.Y.F. Efecto del mineral de ganga en la síntesis de jarosita de potasio y su distribución de tamaños de partículas. *Boletín Miner.* **2006**, *17*, 21–28. (In Spanish)
40. Roca, A.; Patiño, F.; Rivera, I.; Hernández, L.; Pérez, M.; Salinas, E.; Reyes, M. Decomposition and Cyanidation Kinetics of the Argentian Ammonium Jarosite in NaOH Media. *J. Mex. Chem. Soc.* **2007**, *51*, 47–54.